Isomeric states in neutron-deficient $A \sim 80$–90 nuclei populated in the fragmentation of ^{107}Ag

A. B. Garnsworthy,[1,2,*] P. H. Regan,[1] S. Pietri,[1] Y. Sun,[3] F. R. Xu,[4] D. Rudolph,[5] M. Górska,[6] L. Cáceres,[6,7] Zs. Podolyák,[1] S. J. Steer,[1] R. Hoischen,[5,6] A. Heinz,[2] F. Becker,[6] P. Bednarczyk,[6,8] P. Doornenbal,[6] H. Geissel,[6] J. Gerl,[6] H. Grawe,[6] J. Gręboszz,[6,8] A. Kelic,[6] I. Kojouharov,[6] N. Kurz,[6] F. Montes,[6] W. Prokopwicz,[6] T. Saito,[6] H. Schaffner,[6] S. Tachenov,[6] E. Werner-Malento,[9,†] H. J. Wollersheim,[6] G. Benzoni,[10] B. Blank,[11] C. Brandau,[1] A. M. Bruce,[12] F. Camera,[10] W. N. Catford,[1] I. J. Cullen,[1] Zs. Dombrádi,[13] E. Estevez,[14] W. Gelletly,[1] G. Ilie,[15,16] J. Jolie,[15] G. A. Jones,[1] A. Jungclaus,[7,17] M. Kmiecik,[8] F. G. Kondev,[18] T. Kurtukian-Nieto,[14] S. Lalkovski,[12,19] Z. Liu,[1] A. Maj,[8] S. Myalski,[8] M. Pfützner,[9] S. Schwertel,[20] T. Shizuma,[1,21] A. J. Simons,[1,22] P. M. Walker,[1] and O. Wieland[10]

[1]*Department of Physics, University of Surrey, Guildford, Surrey GU2 7XH, United Kingdom*
[2]*WNSL, Yale University, New Haven, Connecticut 06520, USA*
[3]*Department of Physics, Shanghai Jiao Tong University, Shanghai 200240, People's Republic of China*
[4]*Department of Technical Physics, Peking University, Beijing 100871, People's Republic of China*
[5]*Department of Physics, Lund University, S-22100 Lund, Sweden*
[6]*GSI, D-64291 Darmstadt, Germany*
[7]*Departmento di Teórica, Universidad Autonoma de Madrid, E-28050 Madrid, Spain*
[8]*The Institute of Nuclear Physics, PL-31-342 Kraków, Poland*
[9]*IEP, Warsaw University, PL-00-681 Warsaw, Poland*
[10]*Universitá degli Studi di Milano and INFN Milano, I-20133 Milano, Italy*
[11]*CENBG, F-33175 Gradignan Cedex, France*
[12]*School of Environment and Technology, University of Brighton, Brighton BN2 4GJ, United Kingdom*
[13]*Institute of Nuclear Research, H-4001 Debrecen, Hungary*
[14]*Universidad de Santiago de Compostela, E-15705 Santiago de Campostela, Spain*
[15]*IKP, Universität zu Köln, D-50937 Köln, Germany*
[16]*National Institute of Physics and Nuclear Engineering, Bucharest, Romania*
[17]*Instituto de Estructura de la Materia, CSIC, Serrano, E-28006 Madrid, Spain*
[18]*Nuclear Engineering Division, Argonne National Laboratory, Argonne, Illinois 60439, USA*
[19]*Faculty of Physics, University of Sofia "St. Kliment Ohridsk" Sofia, Bulgaria*
[20]*Physik Department E12, Technische Universität München, D-80290 München, Germany*
[21]*Japan Atomic Energy Agency, Kyoto 619-0215, Japan*
[22]*Atomic Weapons Establishment, Aldermaston, Berkshire RG7 4PR, United Kingdom*

(Received 3 July 2009; published 7 December 2009)

The relativistic projectile fragmentation of a 750 MeV per nucleon beam of ^{107}Ag was used to populate isomeric states in neutron-deficient nuclei around $A = 80$–90. Reaction products were separated and unambiguously identified using the GSI FRagment Separator (FRS) and its ancillary detectors. At the final focal plane, the fragments were slowed from relativistic energies by means of an aluminium degrader and implanted in a passive stopper in the center of the high-efficiency, high-granularity Stopped Rare Isotope Spectroscopic INvestigation at GSI (RISING) germanium array. This allowed the identification of excited states in the $N = Z$ nuclei $^{86}_{43}$Tc and, for the first time, $^{82}_{41}$Nb. Isomeric states have also been identified for the first time in ^{87,88}Tc, and a previously unreported isomer was observed in ^{84}Nb. Experimental results are presented along with a discussion on the structure of these nuclei based on interpretations provided by several theoretical models.

DOI: 10.1103/PhysRevC.80.064303 PACS number(s): 29.30.Kv, 23.20.Lv, 23.35.+g, 27.50.+e

I. INTRODUCTION

The region of nuclei close to the $N = Z$ line between ^{56}Ni and ^{100}Sn is a region containing a diverse mixture of nuclear structure features. A low density of single-particle energy levels between the spherical magic numbers 28 and 50 leads to the appearance of prominent shell gaps at oblate ($N, Z = 34, 36$), spherical (40), and prolate (34, 38) shapes [1]. In nuclei close to $N = Z$, neutrons and protons occupy the same single-particle levels. This feature reinforces the tendency for the nucleus to assume a deformed shape and leads to dramatic shape changes with the addition of only a few nucleons [2] or a few hundred keV of excitation [3]. This situation produces several opportunities for excited nuclear states to become long-lived. Shape isomers are possible in this region [3], and the presence of both low-j ($2p_{1/2}$, $2p_{3/2}$) and high-j ($f_{5/2}$, $g_{9/2}$) orbitals can lead to spin-trap isomeric states [4,5]. Toward the top of the shell, nuclear shapes become softer and the $N = Z$ line moves through a transitional region. The proximity now to the N and $Z = 50$ shell closures also

*Present address: TRIUMF, 4004 Wesbrook Mall, Vancouver, BC, Canada V6T 2A3; garns@triumf.ca
†Present address: Institute of Physics Polish Academy of Science, Al. Lotników 32/46, PL-02-668 Warsaw, Poland.

makes seniority isomers an important consideration [6]. The identification and interpretation of isomeric states in this region can lead to important insights into the wide variety of nuclear structure features at play.

The study of $N \sim Z$ nuclei also has important implications in the understanding of explosive nucleosynthesis in nuclear astrophysics. It has been suggested that in x-ray emitting binary systems, nuclei are synthesized via the rapid proton capture process (rp-process) [7] in which a sequence of proton captures and β decays is responsible for the burning of hydrogen into heavier elements. The rp-process proceeds through the exotic mass region with $N \sim Z$ above ^{56}Ni close to the proton dripline. Modern reaction network calculations [8] have suggested that the rp-process can extend up to the heavy Sn-Te mass region, involving nuclei of interest in the current study. Because the detailed reaction rates depend sensitively on the nuclear structure, any information on the low-energy levels of relevant nuclei is potentially of significant importance for such calculations [9].

Projectile fragmentation provides a viable mechanism with which to populate nuclei far from the valley of stability. Long-lived nuclear states present the opportunity to study excited states and structure in exotic nuclei. Several studies involving the fragmentation of heavy ion beams of ^{92}Mo [10], ^{106}Cd [11,12], and ^{112}Sn [13,14] have been carried out to study $N \approx Z$ nuclei between $A = 80 \rightarrow 100$. This article presents experimental results of isomer spectroscopy performed on nuclei populated after the fragmentation of ^{107}Ag projectiles. The structure of the excited states observed in these nuclei is discussed in the framework of the shell model, projected shell-model (PSM), and configuration-constrained total Routhian surface (TRS) calculations.

II. EXPERIMENTAL DETAILS

The experiment was performed as part of the Rare Isotope Spectroscopic INvestigation at GSI (RISING) project [15], an international collaboration using relativistic projectile fragmentation (or fission) reactions to study many aspects of nuclear structure. In the current experiment, the first of the "Stopped beam" campaign, a primary beam of ^{107}Ag ions with 750 MeV per nucleon was provided by the SIS-18 Synchrotron located at Gesellschaft für Schwerionenforschung (GSI). The beam was incident on a 4-g/cm^2 Be production target. The products from projectile fragmentation reactions were transported to the focal plane of the GSI FRagment Separator (FRS) [16], which was operated in achromatic mode. Each transmitted ion was unambiguously identified by measurements of time-of-flight (TOF), position, and energy loss (ΔE) in a series of beamline detectors whose relative positions are shown schematically in Fig. 1. These parameters, when combined with the magnetic rigidity of the dipole magnets, are used to extract the mass-to-charge ratio, A/q, and Z of the transmitted ions on a particle-by-particle basis. In this $B\rho - \Delta E - B\rho$ identification method (where $B\rho$ means magnetic rigidity), a 3.7 g/cm^2 degrader was used at the central focal plane of the FRS (S2 degrader). Further details of the particle identification analysis can be found in Refs. [16] and [17].

After separation and identification, the ions were slowed in a variable-thickness aluminium degrader (S4 degrader) and brought to rest in a multilayer perspex stopper with a total thickness of 7 mm. This passive stopper is located at the central focus of the Stopped RISING germanium array [17,18]. This high-efficiency, high-granularity array consists of 105 hyper-pure germanium detectors arranged in 15 clusters of seven crystals each. The clusters are arranged in three rings at 51°, 90°, and 129° to the secondary beam axis. Gamma rays emitted in the decay of isomeric states are detected in the array and correlated with the arrival of the associated ion. The array has a singles full photopeak efficiency of 11% at 1.3 MeV [18] without add back, and because of the passive stopper being located in air, the absence of a beam pipe between the decaying nucleus and the detectors leads to a γ-ray singles photopeak efficiency of ~34% at 80 keV (with a perspex stopper).

The XIA digital pulse processors (digital gamma finder) DGF4 are used to process the signals recorded by the germanium detectors [17]. The DGF4 module produces an energy and an absolute time-stamp signal with a time resolution of

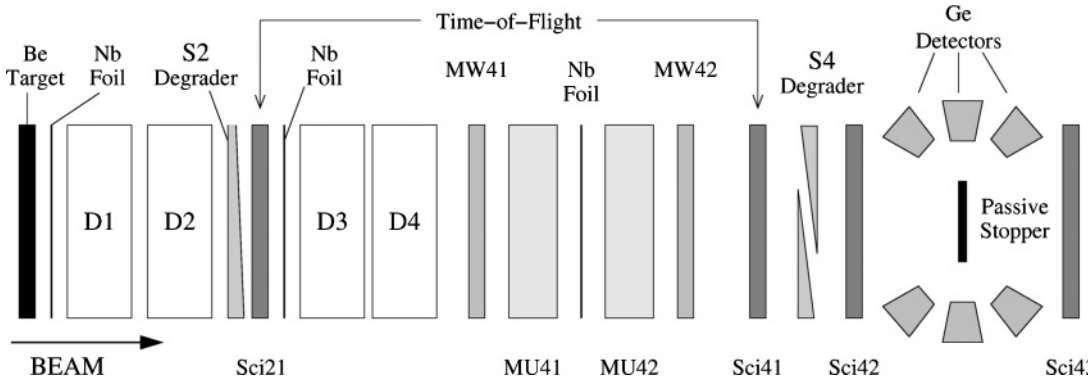

FIG. 1. Schematic outline of the GSI FRS and the suite of beamline detectors used for event-by-event particle identification in the current work. The fragmentation products traverse four dipole magnets (D1–4), two aluminium degraders (S2 and S4), two multiwire proportional counters (MW41,42), two MUSIC (MU41,42), and three scintillators (Sci21,41,42) before coming to rest in a perspex passive stopper at the center of the RISING Stopped Ge array. An additional scintillator (Sci43) is also present after the stopper to veto any ions that do not come to rest there.

TABLE I. Spill structures of the various FRS settings.

Nucleus of central transmission	^{107}Ag ions per spill	Extraction length (s)	Total spill time (s)	Measuring period (h)
^{96}Pd	4×10^6	10	30	16
^{90}Rh	$2–3 \times 10^9$	6	25	5
^{86}Tc	$1–3 \times 10^9$	5–6	25	90
^{82}Nb	2×10^9	5	25	5

25 ns. Two additional analog timing signals are produced by short-range (SR) and long-range (LR) TDCs. These TDCs have 0.293-ns resolution in a total recording period of 850 ns and 0.76-ns resolution in a total recording period of 140 μs, respectively. The start signal for each timing signal comes from a scintillator (Sci41) located immediately before the S4 degrader and before the stopper. The stop signal is provided by the associated Ge crystal.

The magnetic field strength of the dipole magnets of the FRS can be tuned to maximize the transmission of a specific nuclear species. During this experiment, different settings, focused on the fully stripped species of $^{96}_{46}$Pd, $^{90}_{45}$Rh, $^{86}_{43}$Tc, and $^{82}_{41}$Nb, were used. Table I shows the spill structure and measuring period of each setting. The magnetic field strength and S4 degrader thicknesses are shown in Table II. Several nuclear species were transmitted to the focal plane in multiple settings, and in the final analysis, the data from different settings were combined where appropriate.

A. Particle identification and methods of background reduction

The standard particle identification variables are the atomic number, Z, calculated from the energy loss in multisampling ionization chambers (MUSIC) [19], and the mass-to-charge ratio, A/q, determined from measurements of magnetic rigidity and the TOF between Sci21 and Sci41 (Fig. 1). These variables were calibrated using measurements of the primary beam, in this case, ^{107}Ag. Figure 2 shows the identification plot determined by these variables for the combined ^{90}Rh, ^{86}Tc, and ^{82}Nb settings. Gamma-ray spectra associated with delayed events in individual nuclear species can be produced using software coincidence gates on these, and other, particle identification parameters.

Isomeric states that have been previously identified and reported have provided a confirmation of the particle identification and an additional internal calibration of the γ-ray energies, intensities, and timing. Previously reported isomeric decays in ^{94,96}Pd and ^{93}Ru were observed in the current work, and the data obtained are shown in Fig. 3. The half-lives measured for ^{94}Pd and ^{96}Pd in the current work using the digital timing are consistent with those reported in Refs. [20–22].

TABLE II. Magnetic field settings of the dipole magnets of the FRS and the S4 degrader thicknesses used in different settings.

Nucleus of central transmission	D1 (T)	D2 (T)	D3 (T)	D4 (T)	S4 degrader, Al thickness (mg/cm^2)
^{96}Pd	0.73085	0.73284	0.54660	0.54910	1900
^{90}Rh	0.70210	0.70420	0.51880	0.52090	1500
^{86}Tc	0.70015	0.70214	0.52920	0.53150	1900
^{82}Nb	0.70240	0.70460	0.54170	0.54400	2400

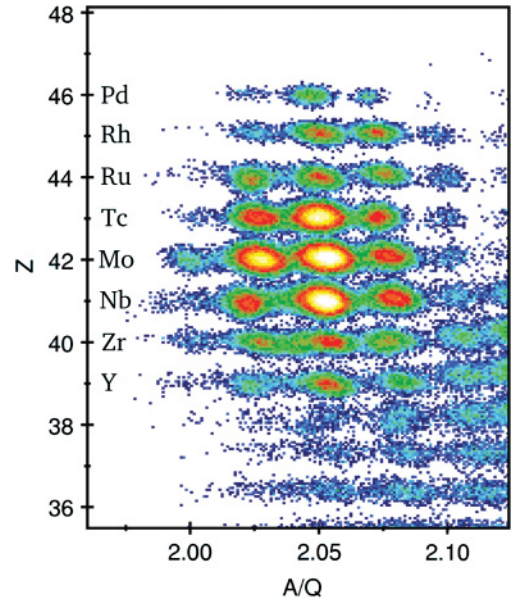

FIG. 2. (Color online) Final, calibrated Z vs. A/q identification plot from the combined ^{90}Rh, ^{86}Tc, and ^{82}Nb settings.

It is worth emphasizing that, with the exception of those for ^{84}Nb, no γ-ray background subtraction has been performed on any of the spectra shown here. The low background in the gamma-ray spectra is achieved by using this event-by-event method of particle identification that provides very sensitive selection of individual nuclear species. The use of appropriate temporal gating highlights specific isomeric decays in the (typically) 100-ns to 100-μs range. The shortest measurable half-lives are limited by the flight time through the separator and by the large background from bremsstrahlung radiation associated with the implantation of the reaction product in the stopper. The longest measurable half-lives are limited by the length of the hardware coincidence window and the time period between implanted ions. The particle identification for γ-ray spectra is improved through additional software gates on combinations of experimental variables to veto events in which fragments undergo subsequent interactions with materials in the beamline. For example, a comparison of the energy loss in the first and second MUSIC chambers can be used to identify and exclude from the analysis ions that undergo reactions in the gas of the MUSIC chambers or the Nb foil between them (upper panel of Fig. 4). Also, fragments that are destroyed in the S4 degrader can be removed by gating on the energy loss in the first MUSIC chamber (MU41) and the energy loss in scintillator 42, which is located immediately after the S4 degrader (lower panel of Fig. 4). A scintillator is also placed after the RISING Stopped array (Sci43) to identify and veto ions that do not come to rest in, or undergo nuclear reactions in, the final stopper.

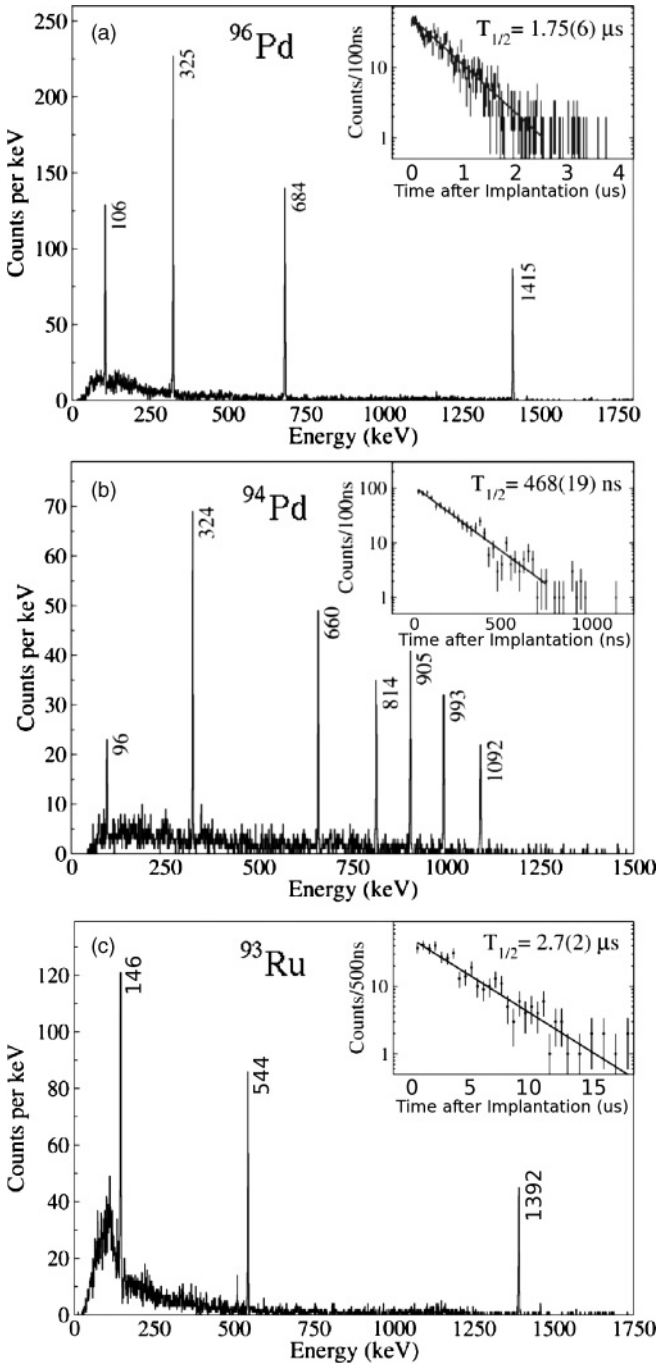

FIG. 3. γ-ray spectra of delayed events associated with ions identified as (a) ^{96}Pd, (b) ^{94}Pd, and (c) ^{93}Ru. The spectra are gated between 150 ns and 5 μs after the time of implantation. The insets show the associated decay curves using a least-squares fit to the DGF timing data.

III. EXPERIMENTAL RESULTS AND DISCUSSION

The primary motivation for the current work was to investigate the low-lying structures in the odd-odd self-conjugate nuclei, ^{82}Nb and ^{86}Tc. Results for these nuclei related to neutron-proton pairing have already been presented in Ref. [23]. Other preliminary results from this work have been presented in a series of conference proceedings [18,24–29].

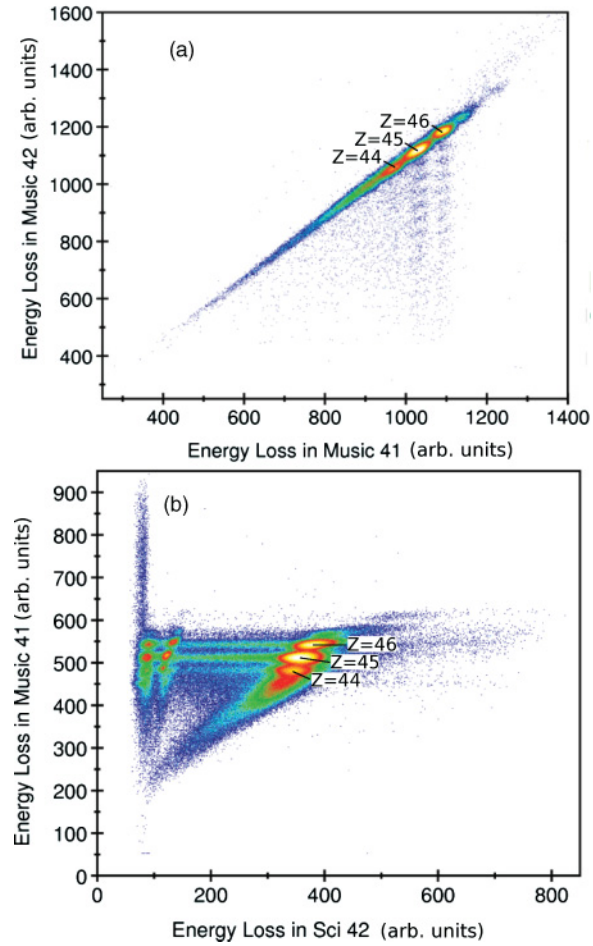

FIG. 4. (Color online) (a) Energy loss in the second MUSIC chamber plotted against energy loss in the first. (b) Energy loss in the first MUSIC chamber plotted against the energy loss in scintillator 42 located immediately after the S4 degrader. Both plots show data collected during the setting focused on ^{96}Pd.

This article reports results from the analysis of the complete data set.

A. Isomeric ratio measurements

The reaction mechanism of projectile fragmentation has been found to populate preferentially the near-yrast states in the product nuclei [30–32]. An isomeric ratio can be defined as the ratio between the number of times a nucleus is populated in that isomeric state and the total number of times that nucleus is produced. Measurements of isomeric ratios can provide insight into both the reaction process and the nature of the observed isomeric states (i.e., an yrast or a nonyrast state). In the current work, the isomeric ratio, R, is defined as in Ref [32] by the expression

$$R = \frac{N_{\text{isomer}}}{N_{\text{ions}} F G}, \tag{1}$$

where N_{isomer} is the number of ions observed in the isomeric state, N_{ions} is the total number of ions of that nuclear species produced, and F and G are correction factors for in-flight losses and for a finite measuring period, respectively. The

number of ions observed in the isomeric state is equal to

$$N_{\text{isomer}} = \sum_i \frac{N_{\gamma_i}}{\epsilon_i} \frac{(1+\alpha_i)}{b_{\gamma_i}}, \tag{2}$$

where N_{γ_i} is the number of γ rays observed in the decay of the ith decay branch depopulating the isomeric state, ϵ_i is the absolute photopeak efficiency of the germanium detectors at that energy, b_γ is the branching ratio of the γ-ray transition, and α_i is the internal conversion coefficient of that γ-ray transition. The correction for in-flight losses is

$$F = \exp\left[-\left(\lambda_{q1}\frac{\text{TOF}_1}{\gamma_1} + \lambda_{q2}\frac{\text{TOF}_2}{\gamma_2}\right)\right], \tag{3}$$

where λ_{qn} is the decay constant for the nucleus in charge state q_n in the first ($n = 1$) and second ($n = 2$) halves of the separator. TOF_1 is the time-of-flight from the production target to the scintillator (Sci21) positioned immediately after the S2 degrader, and TOF_2 is the time-of-flight from Sci21 to Sci41 located immediately before the S4 degrader. γ_n is the corresponding Lorentz factor ($\gamma = \frac{1}{\sqrt{1-(\frac{v}{c})^2}}$). In the mass region of interest here, $A \sim 80$–90, the ions are fully stripped through the full length of the separator so $q_1 = q_2 = Z$. The finite γ-ray measuring time period is accounted for by

$$G = e^{(-\lambda t_i)} - e^{(-\lambda t_f)}, \tag{4}$$

where t_i and t_f are the initial and final measuring times between which the observed isomeric yield is determined. The times are defined with respect to the time of ion implantation in the stopper. Unmeasured losses caused by reaction products being destroyed in the slowing process in the stopper are also taken into account in determining isomeric ratio uncertainties. The isomeric ratios measured in the current experiment are shown in Table III. Also shown are previously reported half-life measurements for comparison that are taken from Refs. [10,21,22,33].

B. $^{82}_{41}\text{Nb}_{41}$

In the work of Chandler *et al.* [10], a short-lived isomeric state was tentatively identified in ^{82}Nb. Low statistics for this nuclide in that experiment prevented the identification of any discrete γ rays or a half-life measurement. The singles spectrum gated on ^{82}Nb ions from the current work is shown in Fig. 5. Three γ rays are now assigned to originate from the decay of this $T_{1/2} = 93(20)$ ns isomeric state [34], and a γ-γ energy coincidence analysis finds all three γ rays to be in mutual coincidence. The level scheme constructed from these data is shown in Fig. 6.

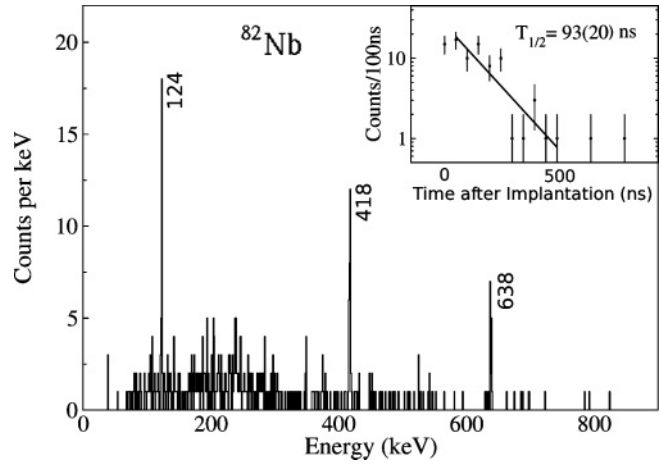

FIG. 5. Singles γ-ray spectrum of delayed events associated with ions identified as ^{82}Nb. The data are gated between 150 and 500 ns after the time of implantation.

The two γ rays at 418 and 638 keV lie close in energy to the $2^+ \rightarrow 0^+$ (407 keV) and $4^+ \rightarrow 2^+$ (634 keV) isobaric analog transitions in ^{82}Zr [35,36]. On this basis, these γ rays are assigned as the first two transitions of the ground-state band in ^{82}Nb. The isomeric state that decays into this band is suggested to have $I = (5)$ based on internal conversion coefficient and transition rate arguments described in detail in Ref. [23].

TRS calculations can be used to predict the deformation and single-particle structure in the vicinity of the Fermi surface in a given nucleus. The configuration-constrained potential-energy-surface calculations developed by Xu *et al.* [37] can predict the deformation for a specific multi-quasiparticle configuration while including the γ degree of freedom. Figure 7 shows a TRS calculation for the ground state of

TABLE III. Isomeric ratios, R, measured in the current experiment. E and J^π refer to the excitation energy, spin, and parity of the isomeric state. The half-lives ($T_{1/2}$) measured in the current work were used to calculate the isomeric ratio quoted. Also shown are previously reported half-life measurements.

Nucleus	E (keV)	J^π	$T_{1/2}$ (this work)	$T_{1/2}$ (other)	R (%)	Number of ions
^{94}Pd	4884	(14^+)	468(19) ns	530(10) ns [21]	28(5)	12721
^{96}Pd	2531	8^+	1.75(6) μs	2.2(3) μs [22]	17(3)	13375
^{93}Ru	2083	$(21/2^+)$	2.7(2) μs	2.20(17) μs [33]	7(1)	44628
^{86}Tc	(1524)	(6^+)	1.10(14) μs	1.11(21) μs [10]	41(7)	7650
^{87}Tc	$71 + x$	$(7/2^+)$	647(24) ns		11(5)	44127
^{88}Tc	95	(4^+)	146(12) ns		6(5)	119298
^{82}Nb	(1180)	(5^+)	93(20) ns		78(77)	4455
^{84}Nb	(48)	(3^+)	176(46) ns		5(2)	240615
^{84}Nb	(305)	(5^+)	50(8) ns		0.5(4)	240615
^{84}Nb	(337)	5^-	92(5) ns	102(19) ns [10]	16(7)	240615

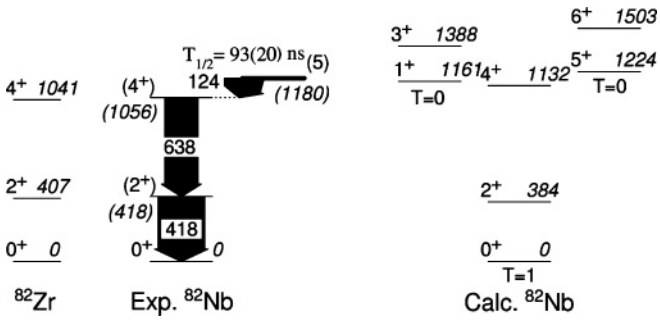

FIG. 6. Experimental level scheme of ^{82}Nb constructed from the current data and results of a PSM calculation. The isobaric analog states in ^{82}Zr are also shown for comparison.

^{82}Nb. The calculation predicts a large stable prolate deformation with $\beta_2 = 0.430$. This compares well with the value of $\beta_2 = 0.41(7)$ in the isobaric analog, ^{82}Zr, which was deduced from the $B(E2 : 2^+ \rightarrow 0^+)$ value and assuming axial symmetry [35,36].

The PSM [38], including neutron-proton (np) interactions [39], has been successful in describing the observed ground-state structures in the even-even $N = Z$ nuclei with $A = 68$ to 88. It was also shown to reproduce well the excited structure in the odd-Z nucleus, ^{83}Nb [40]. In the current work, the PSM has been used to suggest possible configurations for the isomeric state observed in ^{82}Nb. The calculation, for which the positive-parity results are shown in Fig. 6, predicts an $I^\pi = 5^+$ two-quasiparticle state with a Nilsson configuration of $\nu[422]5/2^+ \times \pi[422]5/2^+$ at an excitation energy of 1224 keV. This state is predicted to lie just above the $T = 1$, $I^\pi = 4^+$ state and is a plausible candidate for the configuration of the isomer. The population of a $T = 0$ state with this configuration is consistent with the low-lying

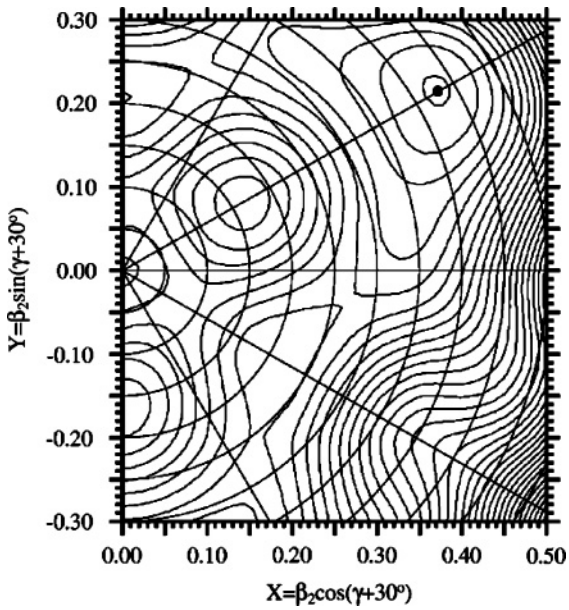

FIG. 7. TRS calculation for the ground state of ^{82}Nb. The minimum is located at $\beta_2 = 0.430$, $\gamma = 0.1^\circ$, and $\beta_4 = -0.023$. The spacing between the contour lines corresponds to 200 keV.

TABLE IV. Calculated partial half-lives derived from the single-particle Weisskopf estimates ($T^W_{1/2}$) [43] and total conversion coefficients [43] of a 124-keV transition in ^{82}Nb.

	124 keV		
	$T^W_{1/2}$ (s)	$\alpha_{\rm tot}$	$T^\gamma_{1/2}$ (s)
$E1$	1.87×10^{-13}	0.065	9.90×10^{-8}
$M1$	1.46×10^{-12}	0.131	1.05×10^{-7}
$E2$	8.97×10^{-7}	0.534	1.43×10^{-7}
$M2$	5.64×10^{-5}	1.120	1.97×10^{-7}

band structures observed in the $T_z = +\frac{1}{2}$ neighbors ^{81}Zr [41] and ^{83}Nb [40,42]. The calculations also predict two low-lying $K^\pi = 4^-$ states at approximately 1.3 MeV (not shown in Fig. 6).

Assuming a dipole transition from the isomeric state, the measured half-life is much greater than the calculated partial half-life shown in Table IV [43]. As discussed in Ref. [23], we attribute this to K hindrance [44], the well-known mechanism by which nuclear half-lives are prolonged in axially well-deformed nuclei. In this particular case of a 124-keV $M1$ $\Delta K = 5$, $\nu = 4$ decay, a reduced hindrance of $f_\nu = (T^\gamma_{1/2}/T^W_{1/2})^{1/\nu} \approx 16$ is intermediate between the accepted f_ν values for the best-case axially symmetric K isomers ($\sim$100) and that of unhindered decays ($\sim$1). An intermediate value is consistent with some degree of K mixing associated with γ-softness, which is supported by predictions from the TRS calculation shown in Fig. 7 and ^{82}Zr [35].

C. $^{84}_{41}$Nb$_{43}$

The first γ-ray transitions assigned to ^{84}Nb were identified by Gross *et al.* [42], where two band structures were observed but were not fitted into a joint level scheme. A further in-beam study by Mărginean *et al.* [45] enabled the construction of a comprehensive level scheme at low excitation energy. In the Mărginean *et al.* study, several rotational bands were identified (including those suggested by Gross *et al.*) and connected to the low-lying structure. The authors noted the confirmation of a previously reported isomeric state, but within their experimental setup, they were unable to measure the half-life or to identify other long-lived states. The isomer reported had been observed in the fragmentation of a ^{92}Mo beam. Preliminary results from the fragmentation study were published in Ref. [46] prior to the work of Mărginean *et al.* The final analysis was published later by Chandler *et al.* [10], where two decay paths depopulating an isomeric state at an excitation energy of 338 keV were reported with a mean lifetime of 148(28) ns. That paper also suggested that a state at 48 keV may have an additional lifetime associated with its decay, but low statistics prevented this from being confirmed.

Our work is in agreement with the findings of Chandler *et al.* [10] and has made it possible to measure the mean lifetime of the 48-keV state. In addition, our work finds that a state at 305 keV reported by Mărginean *et al.* [45] is isomeric. Delayed γ-ray spectra produced from gating on ions

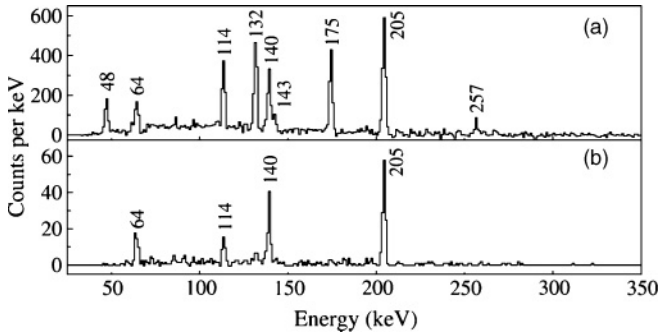

FIG. 8. (a) Singles γ-ray spectra gated on ions identified as ^{84}Nb and a time gate between 200 ns and 1.75 μs. (b) Sum of coincidence energy gates on 132- and 175-keV transitions to highlight the previously observed isomeric decay. Spectrum (b) has the same ion identification and timing conditions as (a).

identified as ^{84}Nb are shown in Fig. 8. Relative intensities of the observed γ rays are shown in Table V along with calculated internal conversion coefficients and single-particle Weisskopf estimates [43]. Because of the short half-life of the isomeric states and the low energy of the transitions in this nucleus, the intensity measured for each γ ray in this case is especially sensitive to the chosen start channel of the time gate. The quoted uncertainty takes this into consideration.

The upper panel of Fig. 8 demonstrates a singles spectrum that in addition to previously reported isomeric transitions shows delayed γ rays at 143 and 257 keV. As our is only sensitive to delayed transitions, these γ rays must decay from a previously unreported isomeric state in ^{84}Nb. These transitions were not observed by Chandler *et al.* [10] but are included in the level scheme reported in the in-beam study [45]. A sum of energy coincidence gates on the 132- and 175-keV direct decays from the previously reported isomeric state is shown in the lower panel and indicates the previously reported decay paths. The 143- and 257-keV transitions, which are shown in the singles spectrum, are too weak to appear in coincidence gating but were identified in Ref. [45] to be depopulating a level at 305-keV excitation energy. The transitions and relative intensities observed in the current work are shown in the level

TABLE V. Relative transition intensities of delayed transitions associated with ^{84}Nb. The intensities have been normalized to the intensity of the 114-keV transition. Also shown are calculated internal conversion coefficients [43] and the single-particle Weisskopf estimate of the assigned multipolarity [43].

E_γ (keV)	$\alpha(M1)$	$\alpha(E1)$	$\alpha(E2)$	$I_{\rm tot}$		$T^W_{1/2}$ (s)
47.9	1.97	1.06	18.0	605(28)	$E2$	1.11×10^{-4}
63.8	0.85	0.46	6.10	98(30)	$E2$	2.57×10^{-5}
114.0	0.16	0.08	0.72	100(19)	$E2$	1.32×10^{-6}
132.4	0.11	0.05	0.42	162(29)	$E2$	6.36×10^{-7}
140.3	0.09	0.04	0.34	89(17)	$E1$	1.28×10^{-13}
143.2	0.09	0.04	0.32	24(4)	$M1$	1.10×10^{-12}
174.8	0.05	0.02	0.15	104(15)	$E1$	6.55×10^{-14}
205.1	0.03	0.02	0.09	156(23)	$E2$	7.04×10^{-8}
257.2	0.02	<0.01	0.04	23(8)	$E2$	2.27×10^{-8}

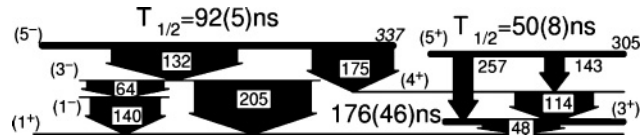

FIG. 9. Proposed level scheme for ^{84}Nb observed in the current work. The widths of the arrows indicate the relative intensities of the transitions.

scheme of Fig. 9. The ground-state spin and parity is taken as 1^+ based on compelling evidence provided in a recent β-decay study of the ^{84}Mo parent [47]. The spin and parity assignment of the 337-keV state is from Ref. [45].

The ordering of the 64- and 140-keV transitions presented in this work is reversed with respect to that in previous publications. This follows the necessary multipolarity assignments made in the current work to satisfy the intensity balance. The original ordering would have resulted in the intermediate state having the same spin/parity as the ground state, and the coexistence of two such states is not justified.

Least-squares fits to the associated decay curves have been made to determine the half-lives of the three isomeric states observed in ^{84}Nb. The fits are shown in Fig. 10. The upper panel is the DGF time spectrum associated with the 132- and 175-keV transitions. The deduced half-life in the current work of 92(5) ns is consistent with the previous measurement by Chandler *et al.* [10] of 102(19) ns.

The 48-keV transition seems to have a longer half-life than the other transitions, which indicates that the 48-keV state is also isomeric. Figure 11 shows the time-difference spectra between the 64- and 140-keV transitions and the 48- and 114-keV transitions. Despite the low coincidence statistics, a significant number of counts appear to the right of the centroid in the lower panel that are absent in the upper. This is an indication that the 48-keV state has a half-life associated with it. Feeding from the 92(5)-ns isomeric state at 337 keV must be taken into account so a two-component least-squares fit has

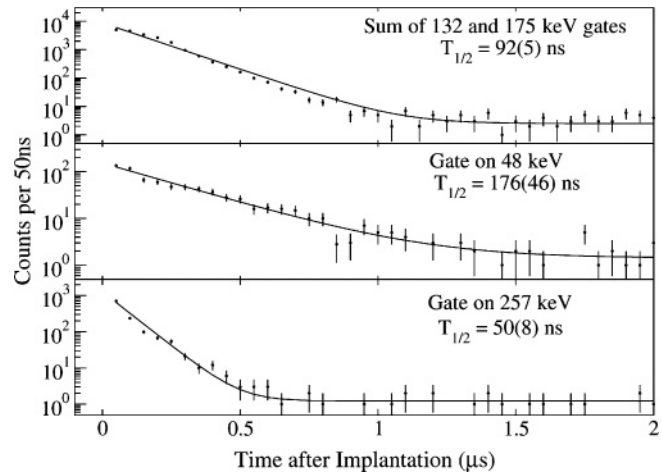

FIG. 10. Half-life measurements from least-squares fits to the DGF timing signal of γ rays associated with the decay of the isomeric states in ^{84}Nb. The decay from the 48-keV isomeric state has been fitted using a two-component least-squares fit assuming feeding from the higher lying, $T_{1/2} = 92(5)$ ns isomeric state.

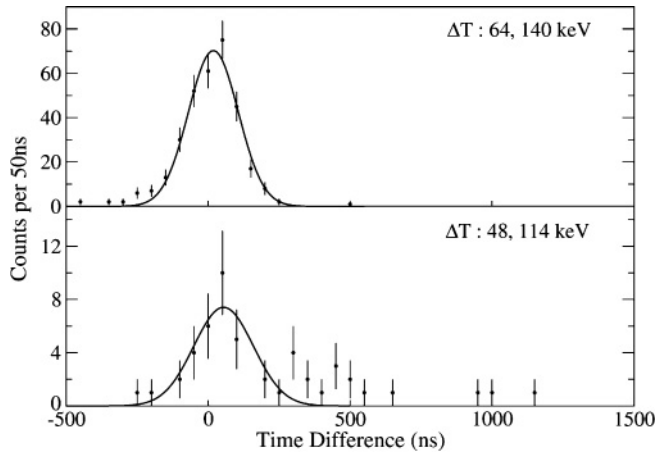

FIG. 11. Time-difference spectra between the 64- and 140-keV transitions (upper panel) and the 48- and 114-keV transitions (lower panel) in ^{84}Nb. The fit assumes no lifetime, so it reflects the time resolution of the setup at these energies. The counts that appear with a large time difference indicate the 48-keV state is isomeric.

been used in this case. The half-life of the 305-keV state has been obtained by a least-squares fit to the 257-keV transition and is found to be 50(8) ns.

D. $^{86}_{43}$Tc$_{43}$

A microsecond isomer in ^{86}Tc was previously reported, and two γ rays tentatively assigned, by Chandler *et al.* [10].

The current work finds five γ rays to be emitted in the decay of a $T_{1/2} = 1.10(14)$ μs isomeric state [34] in ^{86}Tc, as shown in Fig. 12. The measurement of the half-life of this state was made by performing a least-squares fit to the summed time spectra associated with the 593- and 850-keV transitions (inset of Fig. 12). A γ-γ energy coincidence analysis finds the 81-, 593-, and 850-keV γ rays to be in mutual coincidence. These latter two γ rays lie notably close in energy to the $2^+ \rightarrow 0^+$ (567 keV) and $4^+ \rightarrow 2^+$ (761 keV) isobaric analog transitions

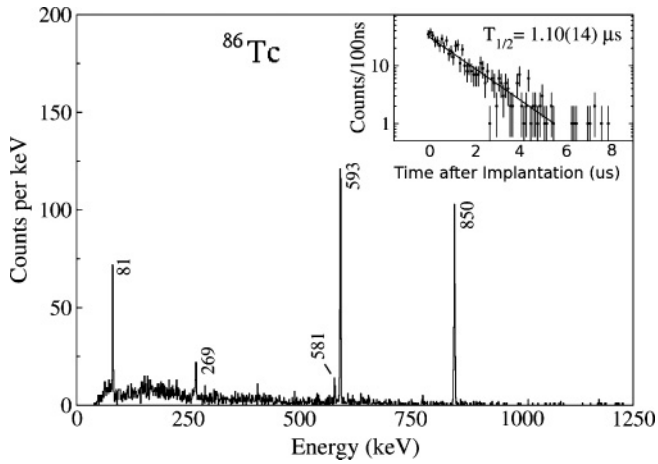

FIG. 12. γ-ray spectra of delayed events associated with ions identified as ^{86}Tc. The data are gated between 150 ns and 5 μs after the time the associated ion arrived in the stopper.

TABLE VI. Calculated γ-ray partial half-lives derived from the single-particle Weisskopf estimates [43] and total conversion coefficients [43] of an 81-keV transition in ^{86}Tc.

	81 keV	
	$T^W_{1/2}$ (s)	$\alpha_{\rm tot}$
$E1$	6.50×10^{-13}	0.245
$E2$	7.08×10^{-6}	2.690
$M1$	3.41×10^{-12}	0.514
$M2$	4.59×10^{-4}	6.420

in $^{86}_{42}$Mo$_{44}$ [48]. On this basis, they are assigned to be the first two transitions of the $T = 1$ ground-state band in ^{86}Tc.

The 269- and 581-keV γ-ray energies sum to 850 keV, which suggests a competing decay branch to the $(4^+) \rightarrow (2^+)$ transition, and this is confirmed in a γ-γ coincidence analysis. The spin and parity of this state is most likely 3^+ or 4^+ when γ-ray selection rules and Weisskopf estimates of the transitions are considered.

An intensity balance around the (4^+) state has been used to infer the conversion coefficient, $\alpha_{\rm tot}$, of the 81-keV γ ray to be 3.49(80). Calculated values of total conversion coefficients for this transition are displayed in Table VI. Good agreement in the current analysis was found for the conversion coefficient of the 96-keV, $14^+ \rightarrow 12^+$, transition in ^{94}Pd, previously reported in Ref. [21]. In our work, this is inferred to be 1.6(3) compared with the previously measured value of 1.9(4) [21] and a theoretical value of 1.61 [43]. On this basis, the 81-keV transition in ^{86}Tc is assigned to be of a stretched-$E2$ multipolarity, leading to a spin/parity assignment of (6^+) for the isomeric state.

The $I^\pi = 6^+$ member of the ground-state band in ^{86}Mo lies at 2260 keV, 932 keV above the 4^+ state. Considering the similarity in energy of the (2^+) and (4^+) members, the $T = 1$, $I^\pi = 6^+$ state in ^{86}Tc would therefore be expected to have an excitation energy of around 2.5 MeV. The isomeric 6^+ state appears at an excitation energy of 1524 keV creating an yrast-trap isomeric state. The fact that this 6^+ state appears only 81 keV above the yrast 4^+ state would explain the somewhat large isomeric ratio (Table III).

The results of a configuration-constrained potential-energy-surface calculation for the ground state in ^{86}Tc are shown in Fig. 13. The minimum for a rotational frequency of $\omega = 0.0$ MeV/$\hbar$ is at $\beta_2 = 0.004$, $\gamma = 0^\circ$. However, if the system is allowed to rotate, then the minimum quickly moves to the triaxially soft, oblate minimum focused around $\beta_2 \approx 0.2$, which is also prominent in Fig. 13. This soft triaxial shape suggests that $N = Z = 43$ represents the boundary along the $N = Z$ line of the transitional region as the doubly magic ^{100}Sn is approached. These findings are in agreement with recent results described by Fischer *et al.* [40].

The positive-parity states in ^{86}Tc predicted by the PSM are shown in Fig. 14. Negative parity states with $K = 5, 6$ are also predicted at $\approx$1.2 MeV. The ground-state band is shown to be well reproduced in the calculation. The $I^\pi = 6^+$ state predicted at 1428 keV is the first excited member of a rotational band built on the $I^\pi = 5^+$ 2-quasiparticle

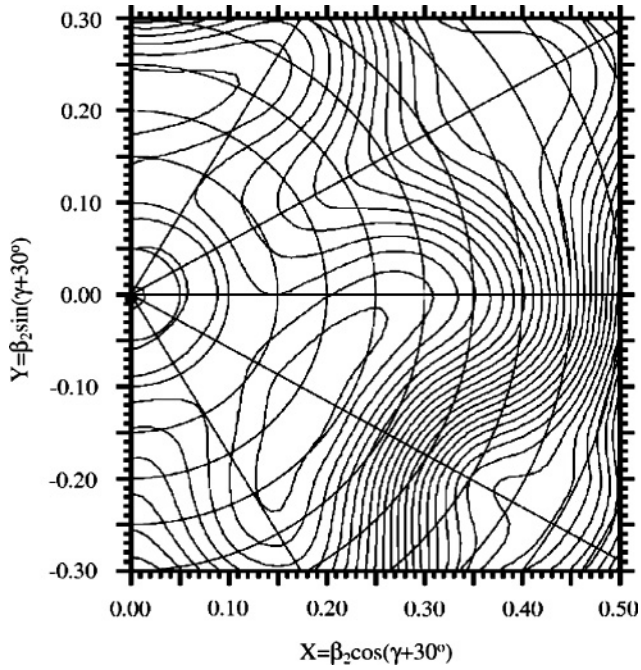

FIG. 13. A configuration-constrained potential-energy-surface calculation for the ground state of ^{86}Tc. The minimum is at $\beta_2 = 0.004$, $\gamma = 0^\circ$ with a shallow oblate minimum around $\beta_2 \approx 0.2$, $\gamma = -60^\circ$, which becomes favored for $\omega > 0$ MeV/$\hbar$. The spacing between the contour lines corresponds to 200 keV.

band head ($\nu[422]5/2^+ \times \pi[422]5/2^+$) and therefore seems unlikely to be isomeric unless rotational alignment brings the 6^+ below the 5^+ state. A more probable configuration for an $I^\pi = 6^+$ isomeric state would be a coupling of the $[413]7/2^+ \times [422]5/2^+$ Nilsson orbitals. Both of these orbitals lie close to the Fermi surface, but the calculation places this state at a significantly higher excitation energy.

It is worth acknowledging an alternative situation in which the isomeric state has $I^\pi = 5^-$ and decays by a mixed $E1/M2$ transition to the (4^+) state. A mixed transition of this type could result in a measured internal conversion coefficient of a similar magnitude to that observed. A mixing ratio of $\delta(E1/M2) = 1.07$ is required for $\alpha_{\rm tot} = 3.49(18)$ matching the measured value or $\delta(E1/M2) = 0.76$, $\alpha_{\rm tot} = 2.47(13)$, to match the calculated pure $E2$ value [49].

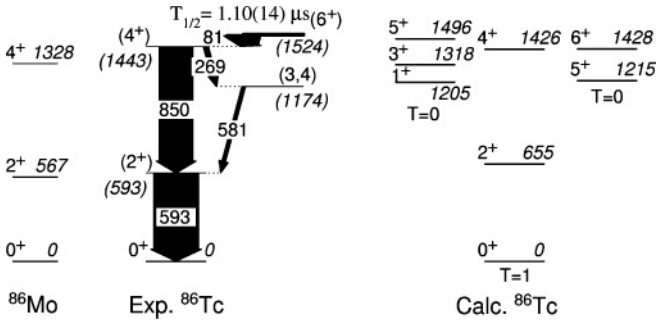

FIG. 14. Experimental and theoretical (PSM) level schemes of ^{86}Tc. The ground-state band of ^{86}Mo is also shown for comparison.

It is also noteworthy that the isomeric state in ^{86}Tc lies in the vicinity of the proton separation energy of 1393(409) keV [50], thus raising the possibility of direct proton emission from the isomer competing with internal γ-ray decay. However, the experimental arrangement used here does not allow us to observe this possible decay mode.

E. $^{87}_{43}$Tc$_{44}$

Two γ rays, likely to form a deformed band built on a proton $g_{9/2}$ state, have been observed in this nucleus previously [51] but no linking transitions to the ground state were identified. The nuclei were produced in fusion-evaporation reactions and studied using prompt spectroscopy. The experimental setup used was only sensitive to γ rays between 0.1 and 2.4 MeV, which were emitted in the first 0.5 ns after production.

Our work identifies two delayed γ rays associated with ^{87}Tc. They can be seen in the singles γ-ray spectrum in Fig. 15. The two transitions of 64 and 71 keV are found to not be in

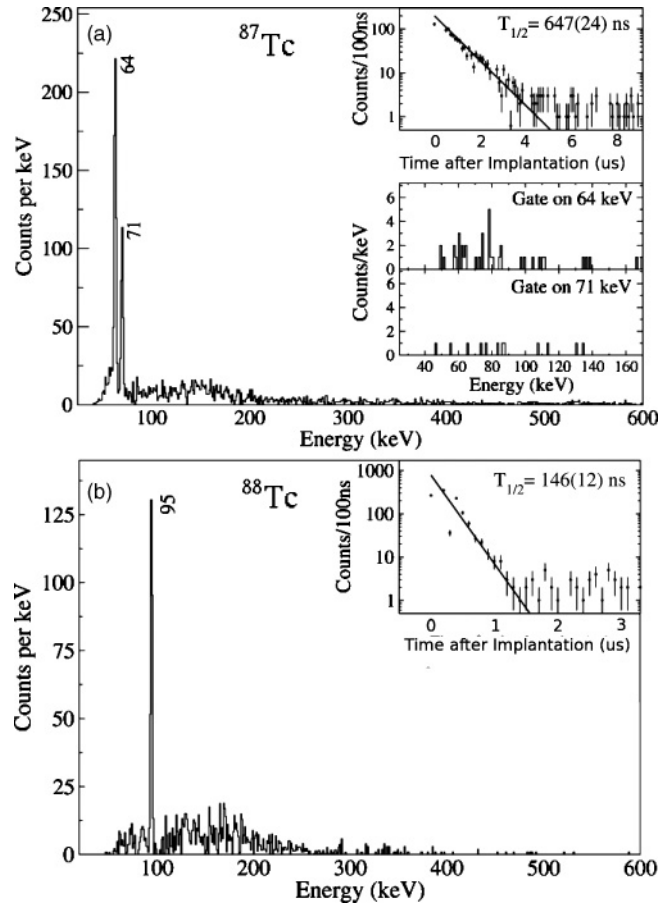

FIG. 15. γ-ray spectra of delayed events associated with ions identified as (a) ^{87}Tc and (b) ^{88}Tc. The spectra are gated from 150 ns to 3.4 μs and from 150 ns to 1.5 μs after implantation, respectively. The insets show the associated decay curves from the DGF timing, and in the case of ^{87}Tc, this is the sum of gates on both the 64- and 71-keV γ rays. The second inset of the upper panel shows energy coincidence gates on the two transitions that are shown to not be in mutual coincidence.

TABLE VII. Calculated partial half-lives for transitions in ^{87}Tc of various multipolarities derived from the single-particle-unit Weisskopf estimates [43]. The units are in seconds.

	7 keV	64 keV	71 keV
$E1$	6.69×10^{-10}	1.31×10^{-12}	9.18×10^{-13}
$E2$	7.42×10^{-1}	2.26×10^{-5}	1.26×10^{-5}
$M1$	3.50×10^{-10}	5.47×10^{-12}	4.32×10^{-12}
$M2$	$4.85 \times 10^{+1}$	1.48×10^{-3}	8.21×10^{-4}

mutual coincidence with each other (inset of Fig. 15). This either constitutes separate decay paths from a single isomeric state or represents the decay of two separate isomeric states in ^{87}Tc. Least-squares fits to the decay curves associated with the individual γ rays finds their half-lives to be the same within experimental uncertainties: 597(33) ns for the 64-keV transition and 680(57) for the 71-keV γ ray. The most likely scenario is therefore a single isomeric state with competing decay paths. A single component half-life fit to the summed decay curve (inset of Fig. 15) gives a half-life measurement of 647(24) ns.

An inspection of the calculated partial half-lives (Table VII) of these observed γ rays indicates that only hindered $E1$ or $M1$ multipolarity can likely result in the observed half-life of the isomeric state. Other multipolarities would result in a much longer lived isomer. $E1$ and $M1$ transitions still require a large degree of hindrance that could be a result of shape hindrance in the decay of an oblate $7/2^+$ ([413]7/2) state to prolate states of $5/2^+$ ([422]5/2) and $5/2^-$ ([303]5/2). All of these single-particle levels lie at the Fermi surface, and similar low-lying structures built on these states have been observed in $N = 43$ isotones [53,54].

F. $^{88}_{43}$Tc$_{45}$

Two β-decaying states with half-lives of 6.4 and 5.8 s have been previously reported in this nucleus [55]. In addition, a quasirotational band was identified during an in-beam study [51] and a partial decay scheme was constructed. It is not clear which β-decaying state, if either, is the ground state of this nucleus or into which state the quasirotational band decays. The new experimental data from our work, combined with theoretical interpretation of these levels, leads to a consistent picture for the low-lying structure of this nucleus.

TABLE VIII. Calculated γ-ray partial half-lives derived from the single-particle Weisskopf estimates and total conversion coefficients of a 95-keV transition in ^{88}Tc [43].

	95 keV	
	$T^W_{1/2}$ (s)	$\alpha_{\rm tot}$
$E1$	3.97×10^{-13}	0.155
$E2$	3.09×10^{-6}	1.520
$M1$	2.48×10^{-12}	0.327
$M2$	2.04×10^{-4}	3.550

In our work, a $T_{1/2} = 146(12)$ ns isomeric state is found to decay via a single 95-keV γ ray as shown in Fig. 15. An inspection of the Weisskopf estimates (Table VIII) suggest either a hindered dipole or an enhanced $E2$ transition.

The results of a shell-model calculation using the Gross-Frenkel interaction [56] in a $1g_{9/2}$-$2p_{1/2}$ model space are shown to the right of Fig. 16. This shell-model space has been shown to consistently perform well for the low-spin, near-spherical states in nuclei with $Z = 40$–45 and $N = 46$–50 [57].

The calculation suggests that the two β-decaying states observed by Odahara *et al.* [55] have spin 2^+ and 6^+ because a low-energy $E4$ transition between these two states is highly unlikely to compete with β decay. In addition, a comparison between the predicted yrast states and the experimental decay scheme strongly suggests $I = 8$ for the X+312 level shown on the left-hand side of Fig. 16. Not only the energy pattern but moreover predicted decay strengths yield a pattern very similar to the observed one (i.e., the 312-keV transition is associated with an $8^+ \rightarrow 6^+$ transition). This implies that the tentative 291-keV transition would be falsely positioned in the experimental decay scheme.

Thus, one is left with two possibilities for a low-energy isomeric transition: either the $4^+ \rightarrow 6^+$ or the $4^+ \rightarrow 2^+$ transition, which means in principle *two* parallel electromagnetic transitions from a possibly isomeric 4^+ level, only one of which is observed in this study. Both the lowest negative-parity states, which are predicted at some 700-keV excitation energy, and odd-spin positive-parity states shown on the right-hand side of

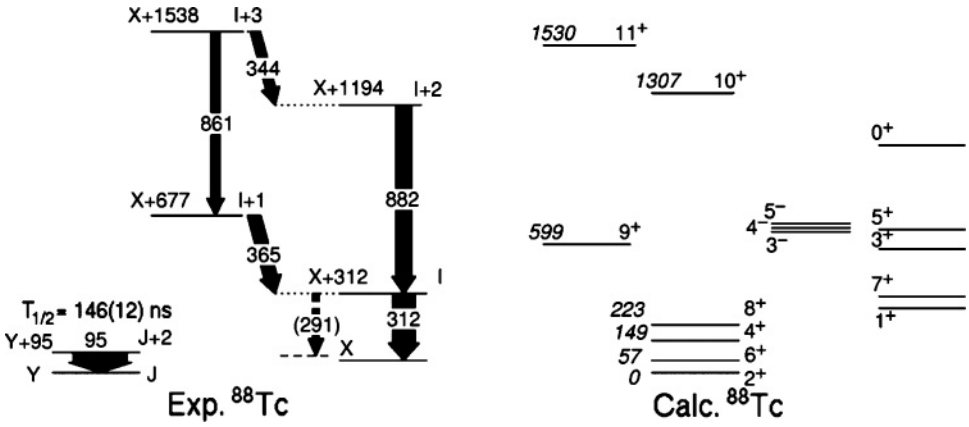

FIG. 16. Experimental and calculated low-spin excitation schemes of ^{88}Tc. The experimental scheme is constructed from the current work (95-keV transition only) and Refs. [55] and [51]. The widths of the arrows indicate relative intensities of the γ rays; the energy labels are in keV, and tentative transitions and levels are dashed. The predictions are based on shell-model calculations in a $1g_{9/2}$-$2p_{1/2}$ model space.

Fig. 16 have open $E1$, $M1$, or $E2$ γ-decay branches of several hundred keV, which precludes these to be isomeric beyond the nanosecond scale.

Assuming the $E2$ character for the observed 95-keV transition, one obtains

$$B(E2)_{\rm exp} = br \times \frac{1}{1+\alpha_{\rm tot}} \times \frac{0.566}{T_{1/2}E_\gamma^5} \sim 200\ e^2\ {\rm fm}^4 \qquad (5)$$

with an experimental branching, $br = 1.0$, $\alpha_{\rm tot} = 1.52(7)$, $T_{1/2} = 146(12)$ ns, and $E_\gamma = 0.095(1)$ MeV. This can be compared with the predictions of $B(E2;4^+ \rightarrow 2^+) = 320\ e^2\ {\rm fm}^4$ and $B(E2;4^+ \rightarrow 6^+) = 7.9\ e^2\ {\rm fm}^4$, respectively, using the effective charges provided for the Gross-Frenkel shell-model interaction [57]. Compared with the experimental number, this clearly points toward matching the observed 95-keV transition with the predicted $4^+ \rightarrow 2^+$ decay, in terms of both excitation energies and, moreover, decay strengths, which would imply $I = 2$ and, most likely, $Y = 0$ keV and $X \sim Y$, on the left-hand side of Fig. 16. This scenario also provides an explanation as to why the $4^+ \rightarrow 6^+$ transition is not seen in the current work and only one isomeric γ-ray transition is observed.

IV. CONCLUSIONS

Experimental results from the first experiment of the RISING "Stopped beam" campaign are reported with a discussion on the structure of these nuclei based on interpretations provided by several theoretical models. These data have allowed the identification of previously unobserved excited states in the self-conjugate odd-odd nuclei ^{82}Nb and ^{86}Tc. The low-lying structures of both systems are dominated by $T = 1$, np pairing effects that have already been observed in the other odd-odd $N = Z$ nuclei above $^{42}_{21}$Sc. The current data suggest that the $T = 1$, rather than the $T = 0$, pairing interaction is the dominant feature throughout the fpg shell [23]. In addition, previously unreported isomeric states have been identified in ^{87}Tc and ^{88}Tc with half-lives of 647(24) ns and 146(12) ns, respectively. These states are interpreted as a shape isomer in ^{87}Tc, and comparison with shell-model calculations finds the (4^+) member of the ground-state band in ^{88}Tc to be isomeric. A previously reported isomeric state in ^{84}Nb has been observed in this data, and another previously identified excited state in this nucleus has now been assigned as isomeric with a half-life of 155(24) ns.

ACKNOWLEDGMENTS

The excellent work of the GSI accelerator and ion source technical staff is gratefully acknowledged. This work was sponsored by the EPSRC (UK) and STFC (UK), The Swedish Research Council, The Polish Ministry of Science and Higher Education (Grant Nos. P03B03030 and N N202 309135), the Bulgarian Science Fund VUF06/05, the US Department of Energy (Grant Nos. DE-FG02-91ER-40609 and DE-AC02-06CH11357), the Spanish Ministerio de Educación y Ciencia (Project Nos. FPA2005-00696 and FPA2007-66069), the German Federal Ministry of Education, the Hungarian Scientific Research Fund (Contract No. K68801), research under Grant No. 06KY205I, and EURONS (European Commision Contract No. 506065). Y.S. acknowledges funding from the Chinese Major State Basic Development Program through Grant No. 2007CB815005 and the Natural Science Foundation of China under Contract No. 10875077. P.M.W. acknowledges funding from the AWE plc. A.B.G. would also like to thank Nexia Solutions Ltd, a subsidiary of BNFL, for financial support.

[1] W. Nazarewicz, J. Dudek, R. Bengtsson, T. Bengtsson, and I. Ragnarsson, Nucl. Phys. **A435**, 397 (1985).
[2] S. Raman, C. W. Nestor Jr., and P. Tikkanen, At. Data Nucl. Data Tables **78**, 1 (2001).
[3] E. Clément *et al.*, Phys. Rev. C **75**, 054313 (2007).
[4] J. Uusitalo, D. Seweryniak, P. F. Mantica, J. Rikovska, D. S. Brenner, M. Huhta, J. Greene, J. J. Ressler, B. Tomlin, C. N. Davids, C. J. Lister, and W. B. Walters, Phys. Rev. C **57**, 2259 (1998).
[5] M. Karny, L. Batist, D. Jenkins, M. Kavatsyuk, O. Kavatsyuk, R. Kirchner, A. Korgul, E. Roeckl, and J. Zylicz, Phys. Rev. C **70**, 014310 (2004).
[6] J. J. Ressler *et al.*, Phys. Rev. C **69**, 034317 (2004).
[7] H. Schatz *et al.*, Phys. Rep. **294**, 167 (1998).
[8] H. Schatz, A. Aprahamian, V. Barnard, L. Bildsten, A. Cumming, M. Ouellette, T. Rauscher, F.-K. Thielemann, and M. Wiescher, Phys. Rev. Lett. **86**, 3471 (2001); H. Grawe, K. Langanke, and G. Martinez-Pinedo, Rep. Prog. Phys. **70**, 1525 (2007).
[9] A. Aprahamian and Y. Sun, Nature Phys. **1**, 81 (2005).
[10] C. Chandler *et al.*, Phys. Rev. C **61**, 044309 (2000).
[11] M. Hencheck *et al.*, Phys. Rev. C **50**, 2219 (1994).
[12] D. J. Morrissey (A1200 Group), Nucl. Phys. **A588**, c203 (1995).
[13] R. Grzywacz *et al.*, Phys. Rev. C **55**, 1126 (1997).
[14] A. Stolz *et al.*, Phys. Rev. C **65**, 064603 (2002).
[15] M. Górska *et al.*, Acta Phys. Pol. B **38**, 1219 (2007).
[16] H. Geissel *et al.*, Nucl. Instrum. Methods Phys. Res. B **70**, 286 (1992).
[17] S. Pietri *et al.*, Nucl. Instrum. Methods Phys. Res. B **261**, 1079 (2007).
[18] S. Pietri *et al.*, Acta Phys. Pol. B **38**, 1255 (2007).
[19] M. Pfützner, H. Geissel, G. Münzenberg, F. Nickel, Ch. Scheidenberger, K.-H. Schmidt, K. Sümmerer, T. Brohm, B. Voss, and H. Bichsel, Nucl. Instrum. Methods Phys. Res. B **86**, 213 (1994).
[20] M. Górska *et al.*, Z. Phys. A **353**, 233 (1995).
[21] R. Grzywacz, in *Proceedings of ENAM, 1998* [AIP Conf. Proc. **455**, 430 (1998)].
[22] H. Grawe and H. Haas, Phys. Lett. **B120**, 63 (1983).
[23] A. B. Garnsworthy *et al.*, Phys. Lett. **B660**, 326 (2008); [Erratum-*ibid.* **B668**, 460 (2008)].
[24] A. B. Garnsworthy *et al.*, Acta Phys. Pol. B **38**, 1265 (2007).
[25] S. Myalski *et al.*, Acta Phys. Pol. B **38**, 1277 (2007).
[26] P. H. Regan *et al.*, Nucl. Phys. **A787**, 491c (2007).
[27] P. H. Regan *et al.*, AIP Conf. Proc. **899**, 19 (2007).
[28] D. Rudolph *et al.*, Eur. Phys. J. Special Topics **150**, 173 (2007).

[29] L. S. Cáceres *et al.*, Acta Phys. Pol. B **38**, 1271 (2007).
[30] Zs. Podolyák *et al.*, Phys. Lett. **B632**, 203 (2006).
[31] K. A. Gladnishki *et al.*, Phys. Rev. C **69**, 024617 (2004).
[32] M. Pfützner *et al.*, Phys. Rev. C **65**, 064604 (2002).
[33] C. M. Baglin, Nucl. Data Sheets **80**, 1 (1997).
[34] The published value for the half-life of this state in Ref. [23] is in fact the value of the mean lifetime. The correct half-life is the one quoted here. All other values quoted or discussed in Ref. [23] were calculated correctly and are not affected by this error.
[35] D. Rudolph *et al.*, Phys. Rev. C **56**, 98 (1997).
[36] S. D. Paul, H. C. Jain, and J. A. Sheikh, Phys. Rev. C **55**, 1563 (1997).
[37] F. R. Xu, P. M. Walker, J. A. Sheikh, and R. Wyss, Phys. Lett. **B435**, 257 (1998).
[38] Y. Sun, Eur. Phys. J. A **20**, 133 (2004).
[39] Y. Sun and J. A. Sheikh, Phys. Rev. C **64**, 031302(R) (2001).
[40] S. M. Fischer *et al.*, Phys. Rev. C **75**, 064310 (2007).
[41] N. Mărginean *et al.*, Phys. Rev. C **69**, 054301 (2004).
[42] C. J. Gross, W. Gelletly, M. A. Bentley, H. G. Price, J. Simpson, B. J. Varley, J. L. Durell, Ö. Skeppstedt, and S. Rastikerdar, Phys. Rev. C **43**, R5 (1991).
[43] F. Rösel, H. M. Friess, K. Alder, and H. C. Pauli, At. Data Nucl. Data Tables **21**, 291 (1978).
[44] K. E. G. Löbner, Phys. Lett. **B26**, 369 (1968); P. M. Walker and G. Dracoulis, Nature (London) **399**, 35 (1999).
[45] N. Mărginean *et al.*, Eur. Phys. J. A **4**, 311 (1999).
[46] P. H. Regan *et al.*, Acta Phys. Pol. B **28**, 431 (1997).
[47] J. B. Stoker *et al.*, Phys. Rev. C **79**, 015803 (2009).
[48] D. Rudolph *et al.*, Phys. Rev. C **54**, 117 (1996).
[49] T. Kibédi, T. W. Burrows, M. B. Trzhaskovskaya, P. M. Davidson, and C. W. Nestor Jr., Nucl. Instrum. Methods Phys. Res. A **589**, 202 (2008).
[50] A. H. Wapstra, G. Audi, and C. Thibault, Nucl. Phys. **A729**, 129 (2003).
[51] D. Rudolph *et al.*, J. Phys. G **17**, L113 (1991).
[52] P. M. Endt, At. Data Nucl. Data Tables **23**, 547 (1979).
[53] N. Mărginean *et al.*, Phys. Rev. C **65**, 034315 (2002).
[54] U. J. Hüttmeier, C. J. Gross, D. M. Headly, E. F. Moore, S. L. Tabor, T. M. Cormier, P. M. Stwertka, and W. Nazarewicz, Phys. Rev. C **37**, 118 (1988).
[55] A. Odahara *et al.*, Z. Phys **354**, 231 (1996).
[56] R. Gross and A. Frenkel, Nucl. Phys. **A267**, 85 (1976).
[57] D. Rudolph, K. P. Lieb, and H. Grawe, Nucl. Phys. **A597**, 298 (1996).